Vol. 15, pp. 165–172 (2018)
doi: 10.2142/biophysico.15.0_165

Biophysics and Physicobiology

https://www.jstage.jst.go.jp/browse/biophysico/

Regular Article

Influence of various parameters in the replica-exchange molecular dynamics method: Number of replicas, replica-exchange frequency, and thermostat coupling time constant

Ryosuke Iwai[1]*, Kota Kasahara[2]* and Takuya Takahashi[2]

[1]*Graduate School of Life Sciences, Ritsumeikan University, Kusatsu, Shiga 525-8577, Japan*
[2]*College of Life Sciences, Ritsumeikan University, Kusatsu, Shiga 525-8577, Japan*

Received March 7, 2018; accepted July 5, 2018

The replica-exchange molecular dynamics (REMD) method has been used for conformational sampling of various biomolecular systems. To maximize sampling efficiency, some adjustable parameters must be optimized. Although it is agreed that shorter intervals between the replica-exchange attempts enhance traversals in the temperature space, details regarding the artifacts caused by these short intervals are controversial. In this study, we revisit this problem by performing REMD simulations on an alanine octapeptide in an implicit solvent. Fifty different sets of conditions, which are a combination of five replica-exchange periods, five different numbers of replicas, and two thermostat coupling time constants, were investigated. As a result, although short replica-exchange intervals enhanced the traversals in the temperature space, they led to artifacts in the ensemble average of the temperature, potential energy, and helix content. With extremely short replica-exchange intervals, i.e., attempted at every time step, the ensemble average of the temperature deviated from the thermostat temperature by *ca.* 7 K. Differences in the ensembles were observed even for larger replica-exchange intervals (between 100 and 1,000 steps). In addition, the shorter thermostat coupling time constant reduced the artifacts found when short replica-exchange intervals were used, implying that these artifacts are caused by insufficient thermal relaxation between the replica-exchange events. Our results will be useful to reduce the artifacts found in REMD simulations by adjusting some key parameters.

Key words: generalized ensemble, conformational sampling, molecular simulation, thermal relaxation, enhanced sampling

Molecular dynamics (MD) simulations are a promising computational approach to investigate the microscopic behavior of molecular systems and have been successfully applied to various problems, e.g., drug discovery [1,2]. Although recent advances in computational technology have extended the scope of MD simulations [3,4], insufficiency of the simulation time scale is still considered a major limitation of this approach. Equilibration of a molecular system with a high degree of freedom requires a long time scale, which cannot be attained by conventional MD methods with current general-purpose computers [5–7].

* The first two authors are considered to be joint first authors.
Corresponding author: Kota Kasahara, College of Life Sciences, Ritsumeikan University, Noji-higashi 1-1-1, Kusatsu, Shiga 525-8577, Japan.
e-mail: ktkshr@fc.ritsumei.ac.jp.

◀ ***Significance*** ▶

The replica-exchange molecular dynamics (REMD) method is a powerful approach to investigate conformational ensembles of molecular systems. Although this method requires some adjustable parameters, there is no golden standard for setting of the parameters. Effects of the parameters on sampling efficiency and resultant ensemble have been argued. Our evaluation found that shorter intervals for replica-exchange attempts enhance conformational sampling but cause the artifacts due to insufficiency of thermal relaxation. In particular, the ensemble average of temperature deviates from the target temperature of the thermostat. The results of this evaluation will be helpful to adjust the parameters for REMD simulations.

To overcome this limitation, a variety of extended ensemble approaches have been extensively developed [8,9]. The replica-exchange MD (REMD) method [10], also known as the parallel tempering MD, is one of the generalized ensemble MD methods. The REMD method consists of performing several constant-temperature MD simulations on the same molecular system at different temperatures and exchanging the temperature of the thermostat between pairs of simulations based on the Metropolis criterion. Each simulation, or replica, traverses a wide range of temperatures, and thus, various molecular conformations can be efficiently sampled. Applying a re-weighting method to the multiple trajectories obtained at different temperatures generates a conformational ensemble in an equilibrium state at a target temperature [11,12]. In the past decades, many variant methods of REMD have been developed, e.g., Hamiltonian REMD [13], surface tension REMD [14], solute tempering [15,16], and mass scaling REMD [17]. REMD-based enhanced conformational sampling methods have been applied to investigate the conformational ensembles of a variety of molecular systems in an equilibrium state [18].

Since a major bottleneck of the REMD method is its high computational cost induced by the parallel computations of many replicas, optimizing the sampling efficiency is essential. In particular, optimizing the values of several adjustable parameters, such as the number of replicas (referred to as N_{rep}, hereafter) and the time interval between the replica-exchange attempts (referred to as t_{att}, hereafter), is not straightforward, and many evaluations of these parameters have been reported. Periole & Mark reported that for the conformational sampling of a heptapeptide with explicit water molecules, a short interval (t_{att}=0.1 ps) resulted in a high frequency of *back exchange* and high autocorrelation of the potential energy [19]. Abraham & Gready also suggested utilizing $t_{att} \geq 1.0$ ps to avoid the autocorrelation of the potential energy [20]. Jani *et al.* simulated the folding–unfolding equilibrium of an engrailed homeodomain with three different combinations of t_{att} and simulation temperature and found that these settings impact the resultant ensembles [21]. On the other hand, Sindhikara *et al.* reported that short t_{att} enhance traversals in the temperature space without side effects based on simulations of short peptides with both implicit and explicit solvents [22,23], and Rosta & Hummer supported this conclusion [24]. Although it is clear that the shorter intervals enhance traversals in the temperature space, the recommended lower limit and artifacts generated are still debated.

Herein, we revisit the evaluation of different REMD parameters using a poly-alanine peptide with an implicit solvent model following the protocol presented by Sindhikara *et al.* [22]. To evaluate the artifacts generated by the short interval between replica-exchange attempts, we tested a wide range of t_{att}, including extremely frequent attempts (t_{att}=0.001, 0.005, 0.01, 0.1, and 1 ps). In addition, we considered five different numbers of replicas (N_{rep}=8, 12, 16, 20, and 32) as well as the thermostat coupling time constant τ, whose effects have not yet been reported. Since the previous study implies that the artifacts caused by short t_{att} arise because of insufficient thermal relaxation between the replica-exchanges [19], τ should have a key role. In total, 5×5×2=50 sets of REMD simulations were performed to assess the effects of these three adjustable parameters on the resultant ensemble and on the sampling efficiency. The obtained ensembles were characterized by the helix content, potential energy distribution, and temperature distribution. The simulation time required for a round trip in the temperature space was assessed to evaluate the sampling efficiency. As a result, though shorter t_{att} enhance traversals in the temperature space, which is consistent with the previous works, they also tend to generate artifacts in the ensembles. In addition, longer τ caused more significant artifacts for shorter t_{att}. This result encourages the use of longer t_{att} to minimize artifacts, and there is therefore a trade-off between the accuracy of the ensemble and the sampling efficiency.

Methods

Simulation Settings

The REMD simulations were performed on a poly-alanine octapeptide with an implicit solvent model under various conditions (t_{att}, N_{rep}, and τ). As the initial structure for all simulations, an ideally extended structure of the poly-alanine octapeptide was built using the *tLEaP* software included in the AMBER suite. The N- and C-termini were capped with acetyl and N-methyl groups, respectively. For the potential calculations, the AMBER parm99SB force field [25] and the generalized Born (GB) implicit solvent model with the OBC(II) parameter [26] were utilized. The cut-off distance was large enough to cover the entire system. Covalent bonds involving hydrogen atoms were constrained by using the LINCS method [27,28]. The integration time step (Δt) was 1.0 fs. The Nosé–Hoover thermostat [29,30] was applied to generate *NVT* ensembles. The target temperature of each replica was defined as a geometric series ranging from 300 to 800 K.

We performed REMD simulations with 50 sets of conditions; *i.e.*, the combination of five time intervals between replica-exchange attempts (t_{att}=0.001, 0.005, 0.01, 0.1, and 1 ps), five total number of replicas (N_{rep}=8, 12, 16, 20, and 32), and two coupling time constants for the Nosé-Hoover thermostat (τ=0.2 and 2 ps). The simulation time was 10 ns for each replica following the previous evaluation by Sindhikara *et al.* [22]. In total, 8.8 μs of REMD simulations were examined. All the simulations were performed using the Gromacs (ver. 4.6.1) software [31] with a modification for the velocity-rescaling of the thermostat [32]. In order to analyze the raw distribution at each thermostatting temperature, we did not apply re-weighting methods, e.g., the weighted histogram analysis [11] and multistate Bennett acceptance ratio methods [12].

Definitions

Herein, several parameters are used to describe the structural ensembles and simulation conditions. This sub-section summarizes all the terms used in this paper.

The adjustable parameters for the REMD simulations are t_{att}, N_{rep}, T_k, and τ. t_{att} denotes the time interval between replica-exchange attempts. N_{rep} is the number of replicas. T_k is the target temperature of the k-th thermostat, where $k=1, 2, ..., N_{rep}$. τ represents the coupling time constant for the Nosé–Hoover thermostat. The REMD simulations were characterized by the parameters P_{acc}, t_{acc}, t_{round}, F_H, F_G, R_g, T, and V. P_{acc} denotes the acceptance ratio of the replica-exchange attempts. t_{acc} is the expected time for accepting the replica-exchange attempts, calculated as $t_{acc}=t_{att}/P_{acc}$. t_{round} is the time required for a round trip in the temperature space; the round trip is defined as the traversals from a lowest/highest temperature ($k=1$ or $k=N_{rep}$) to a highest/lowest and back to the initial (lowest/highest) temperature. F_H and F_G indicate the ensemble average of fraction of α- and 3_{10}-helices in an ensemble at 300 K, respectively. These secondary structural elements were assessed using the DSSP software [33], and the fractions were calculated as the ratio of the number of residues with a given secondary structural element to the total number of residues. The radius of gyration (R_g) is measured with the *g_gyrate* module of the Gromacs package. T and V are the temperature and potential energy, respectively, of a sampled snapshot. The operators $< >$ and $\sigma(\ )$ denote the average and standard deviation, respectively. In particular, the statistics over an ensemble at the k-th temperature are described as $< >_k$ and $\sigma(\ )_k$.

Results and Discussion

The first three sub-sections describe the results for $\tau=2.0$ ps. The first sub-section, *Traversals in temperature space*, discusses the sampling efficiency of the REMD simulations in terms of the time required for a round trip in the temperature space. The characteristics of the resultant ensembles are discussed in the second and third sub-sections, *Helix content and radius of gyration* and *Potential energy and temperature distributions*, respectively. The differences between the simulations for $\tau=2.0$ and 0.2 ps are discussed in the fourth sub-section, *Effects of the thermostat coupling constant*.

Traversals in temperature space

For the REMD simulations with $\tau=2.0$ ps and combinations of t_{att} and N_{rep}, the sampling efficiencies were assessed in terms of the average time for a round trip in the temperature space (t_{round}; Table 1). In general, the shorter t_{att} exhibited faster traversals in the temperature space, consistent with previous reports [22,23]. In addition, for each time interval t_{att}, a distinct highest-efficiency value of N_{rep} was observed; the N_{rep} values that exhibit the fastest round trips for each t_{att} were 32, 16, 12, 12, and 12 for $t_{att}=0.001$, 0.005, 0.01, 0.1, and 1 ps, respectively. The most efficient N_{rep} value tends to decrease with an increase in t_{att} and reaches a plateau at $t_{att}\geq0.01$ ps. Although the larger N_{rep} showed higher acceptance ratios owing to larger overlaps of the energy distribution between neighboring replicas (Table 2), the larger N_{rep} require larger number of acceptances for a round trip. Thus, unless extremely frequent replica-exchange attempts were performed, the higher N_{rep} did not show better performance. An acceptance ratio of $P_{acc}\sim0.5$ seems to be the best condition for $t_{att}\geq0.01$ ps. Note that since P_{acc} depends on the

Table 1 The acceptance ratio for replica-exchange attempts, P_{acc}

	τ	2	2	2	2	2	0.2	0.2	0.2	0.2	0.2
N_{rep}	t_{att}	1	5	10	100	1000	1	5	10	100	1000
8		0.257	0.236	0.253	0.247	0.249	0.259	0.234	0.253	0.246	0.249
12		0.470	0.446	0.471	0.464	0.466	0.472	0.448	0.471	0.462	0.465
16		0.597	0.578	0.599	0.587	0.591	0.597	0.579	0.600	0.590	0.592
20		0.674	0.662	0.679	0.669	0.669	0.675	0.663	0.679	0.670	0.672
32		0.790	0.791	0.798	0.795	0.795	0.791	0.791	0.798	0.795	0.796

Table 2 Average time for a round trip in the temperature space, t_{round} (ps)

	τ	2	2	2	2	2	0.2	0.2	0.2	0.2	0.2
N_{rep}	t_{att}	1	5	10	100	1000	1	5	10	100	1000
8		38.47	82.02	81.36	204.95	983.39	17.33	36.82	52.65	198.77	777.28
12		33.77	62.05	69.95	199.36	680.41	14.96	34.94	45.44	202.64	797.09
16		33.06	59.78	74.86	219.64	829.89	16.57	35.38	46.39	195.76	859.40
20		33.21	64.18	78.60	219.28	857.71	17.50	37.48	54.94	210.11	890.37
32		28.37	65.33	84.64	279.36	999.38	16.53	42.73	63.03	257.33	1102.94

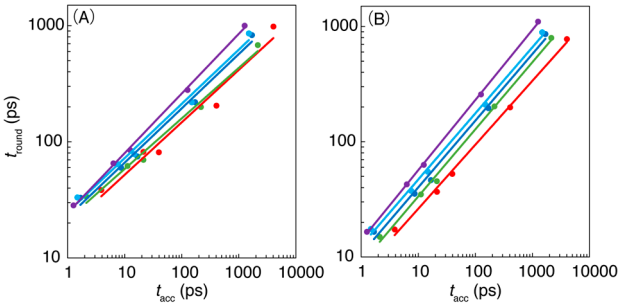

Figure 1 Relationship between the expected time for an acceptance (t_{acc}; the horizontal axis) and the average time required for a round trip in the temperature space (t_{round}; the vertical axis) with (A) τ=2 ps and (B) τ=0.2 ps. The conditions N_{rep}=8, 12, 16, 20, and 32 are shown in red, green, blue, cyan, and purple, respectively. The lines indicate least-square fitted functions.

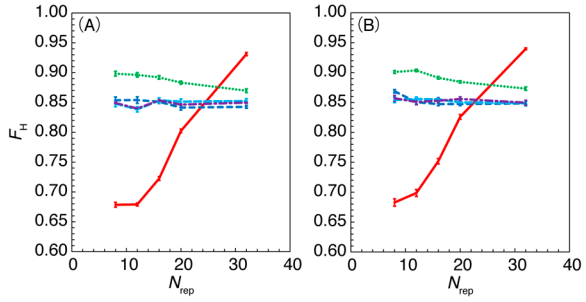

Figure 2 α-helix content in the resultant ensembles with (A) τ=2 ps and (B) τ=0.2 ps. The horizontal and vertical axes indicate N_{rep} and F_H, respectively. The conditions t_{att}=0.001, 0.005, 0.01, 0.1, and 1 ps are shown in red, green, blue, cyan, and purple, respectively. The error bars indicate the standard errors among 20 sub-trajectories generated by uniformly dividing the last 9 ns of the original trajectory.

degree of freedom of the system, the most efficient conditions can vary for different systems.

Regarding the expected time to accept a replica-exchange attempt, log(t_{acc}) was proportional to log(t_{round}) for each value of N_{rep} (Fig. 1). In addition, the larger N_{rep} tended to cause longer t_{round} for the same t_{acc} because of the larger acceptance number required for a round trip.

Helix content and radius of gyration

The fractions of α-helix conformations (F_H) in the ensembles at 300 K are summarized in Figure 2. The three longest intervals between replica-exchange attempts ($t_{att}\geq$0.01 ps) exhibited similar F_H values regardless of the number of replicas (F_H=0.838~0.854). On the contrary, when t_{att}=0.001 ps, larger N_{rep} resulted in higher F_H. Although the F_H values when t_{att}=0.005 ps also depended on N_{rep}, the trend was the opposite (smaller N_{rep} resulted in lower F_H), and the deviations of the F_H values with respect to those obtained with longer t_{att} were subtle. In particular, when t_{att}=0.005 ps and N_{rep}=32, the fraction of α-helix conformations (F_H=0.870) was similar to those with longer t_{att}. While the three longest intervals ($t_{att}\geq$0.01 ps) exhibited similar F_H values, subtle differences were observed; the Pearson correlation coefficient (PCC) of the F_H values for the five N_{rep} conditions between t_{att}=0.01 and 1 ps was –0.187 and that between t_{att}=0.1 and 1 ps was 0.902. These results indicate that t_{att} has a significant impact on the conformational ensemble, and longer t_{att} produce more robust resultant ensembles in terms of F_H with a wide range of N_{rep}. The effects of t_{att} on F_H converged when $t_{att}\geq$0.1 ps. Note that the 3_{10}-helix content, F_G, was negatively correlated with F_H (the PCC between F_H and F_G was –0.99; Supplementary Fig. S1).

An experimental study of a poly-alanine heptapeptide suggested that the poly-proline II conformation was the dominant structure [34], which is inconsistent with our simulation results that indicate high helix tendencies (F_H~0.85). However, a direct comparison with experimentally measured helix contents is not straightforward because of the limitation of the current force fields and implicit solvent models [35]. Even with explicit solvent models, the radius of gyration of denatured peptides tends to be underestimated by some standard force fields [36,37], and issues caused by finite-size effects arising from the periodic boundary conditions have also been raised [38–41]. In addition, experimental quantification of helix content of oligopeptides is not straightforward [42]. Nevertheless, this study focuses only on the relative differences among the REMD configurations, and consistency with experimental measurements is out of the scope of this work.

We also analyzed the peptide conformations in terms of R_g and found that R_g was negatively correlated with F_H (PCC was –0.99; Supplementary Fig. S2). In addition, we confirmed the convergence of R_g by calculating its cumulative average as a function of the simulation time (Supplementary Fig. S3). R_g values converged in the simulation time, and there were no clear differences among simulations carried out using various REMD conditions.

Potential energy and temperature distributions

We evaluated the potential energy and temperature distributions of the simulated ensembles at the lowest temperature (T_1=300 K). For t_{att}=0.001 ps, the potential energy distribution is shifted compared with the other four t_{att} values; smaller and larger N_{rep} showed higher and lower potential energies, respectively (Fig. 3A, B and Supplementary Fig. S4A, B, C). The difference in the ensemble averages of the potential energy $\langle V\rangle_1$ with the different parameters showed a trend similar to the α-helix content (F_H); the PCC between $\langle V\rangle_1$ and F_H was –0.99 (Figs. 2A and 3C).

For the temperature distribution, the most significant shift was observed for t_{att}=0.001 ps with N_{rep}=32 (Fig. 4B). Its ensemble average of temperature $\langle T\rangle_1$ was 293.13 K despite that the target temperature of the thermostat was 300 K. Contrarily to the potential energy distribution, no clear shift of the temperature distribution was observed for N_{rep}=8 with t_{att}=0.001 ps (Fig. 4A); the distributions obtained for the

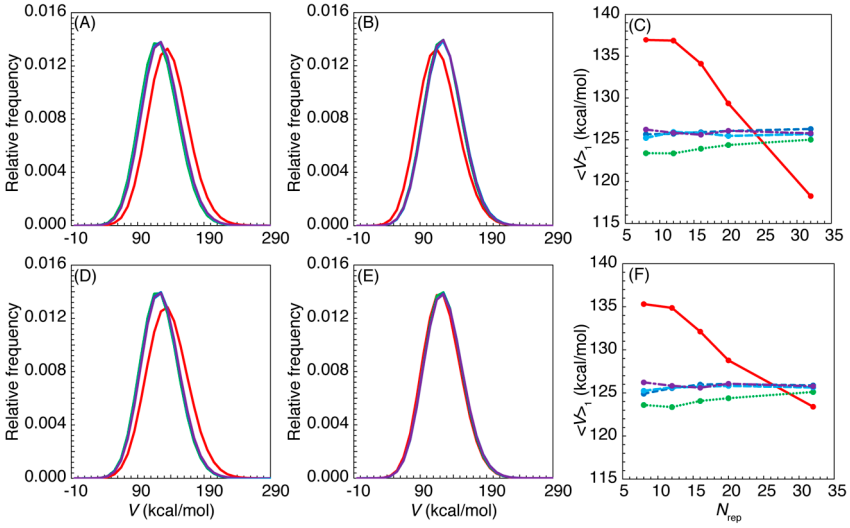

Figure 3 Potential energy distributions in ensembles at 300 K with (A, B, C) τ=2 ps and (D, E, F) τ=0.2 ps. The conditions t_{att}=0.001, 0.005, 0.01, 0.1, and 1 ps are shown in red, green, blue, cyan, and purple, respectively. (A, B, D, E) The distribution of the potential energy V in each ensemble are shown for (A, D) N_{rep}=8 and (B, E) N_{rep}=32. (C, F) Ensemble averages of the potential energy $<V>_1$ for each N_{rep} and t_{att} conditions are summarized.

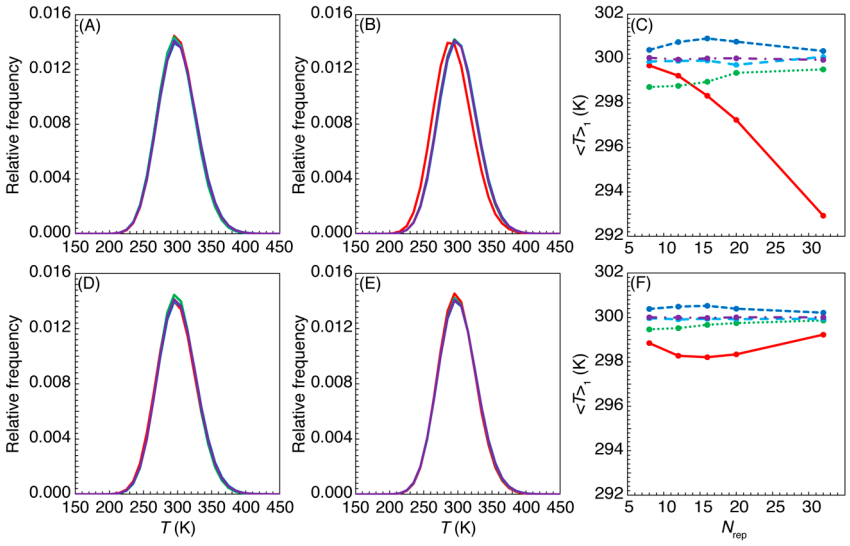

Figure 4 Temperature distributions in ensembles at 300 K with (A, B, C) τ=2 ps and (D, E, F) τ=0.2 ps. Notations are the same with Figure 3. (A, B, D, E) The distribution of the temperature T in each ensemble are shown for (A, D) N_{rep}=8 and (B, E) N_{rep}=32. (C, F) Ensemble averages of the temperature $<T>_1$ for each N_{rep} and t_{att} conditions are summarized.

other N_{rep} values are shown in Supplementary Figure S5A, B, C. The ensemble averages of temperatures $<T>_1$ for various conditions are summarized in Figure 4C. This clearly shows that there is a problem if the frequency of the replica-exchange attempts is very high (t_{att}=0.001 ps); at this value, the ensemble average of temperatures exhibited a distinct behavior and largely deviated from the target temperature of the thermostat. For longer t_{att}, the deviations from the target temperature were smaller; the maximum errors from the target temperature were 7.07, 1.28, 0.91, 0.28, and 0.06 K for t_{att}=0.001, 0.005, 0.01, 0.1, and 1 ps, respectively. It is noteworthy that there were detectable differences even between the two largest t_{att} values.

Thermostatting errors were also observed in replicas with higher temperatures. The ratios of the ensemble average of the temperature over the target temperature $<T>_k/T_k$ for various conditions are summarized in Figure 5 and Supplementary Figure S6. Interestingly, these ratios oscillated along the temperature index, k. In general, the ratios of the $(k+2i)$-th temperatures, where k and i denote positive integers, were similar. This zigzag profile was common, irrespective of N_{rep}, and the wavelength of the oscillation (of the tem-

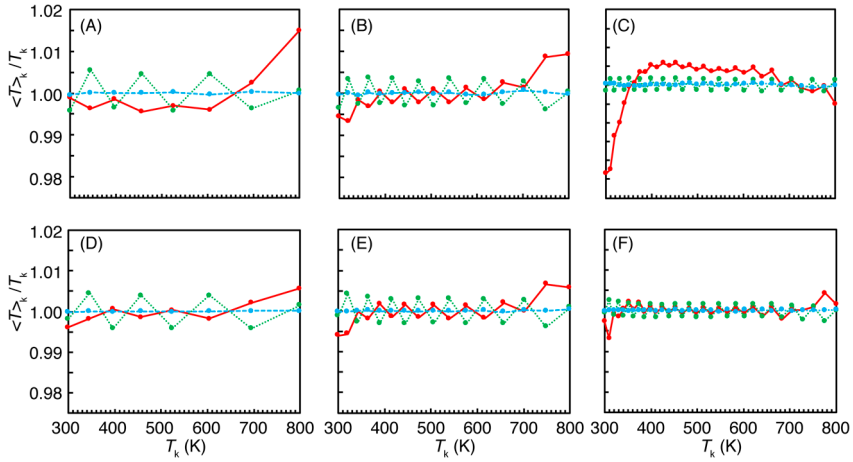

Figure 5 Ratios of the ensemble average of temperatures to the target temperature at *k*-th thermostat $<T>_k/T_k$ with (A, B, C) τ=2 ps and (D, E, F) τ=0.2 ps for each N_{rep} condition: (A, D) N_{rep}=8 , (B, E) N_{rep}=16, and (C, F) N_{rep}=32. The results with for t_{att}=0.001, 0.005, and 0.1 ps are shown in red, green and cyan, and those with t_{att}=0.01 and 1 ps are not shown for clarity.

perature) was always equal to two replicas. This artificial oscillation tended to decay with an increase in t_{att}. We speculate that this oscillation is due to the REMD protocol, which performs two types of replica-exchange attempts consecutively: (i) exchanging the 1st–2nd, 3rd–4th, ... replica pairs and (ii) exchanging the 2nd–3rd, 4th–5th, ... replica pairs. If the system temperature is not properly relaxed in the time interval between the replica-exchange attempts, such a systematic trial scheme can generate the oscillation.

Effects of the thermostat coupling constant

The coupling constant τ of the Nosé–Hoover thermostat is one of the key parameters of MD simulations. We examined the effects of τ by performing REMD simulations with two settings, τ=0.2 and 2 ps. First, the shortest τ enhanced traversals in the temperature space (Table 2), but τ did not affect the acceptance ratio of the replica-exchange attempts P_{acc} (Table 1). This behavior can be interpreted as follows. After a replica-exchange attempt is accepted, the two exchanged replicas should have similar temperatures. When successive replica-exchange attempts occur before thermal relaxation, the attempts to move these replicas to the previous temperature should have high acceptance probabilities. Namely, a longer τ, indicative of a slower thermal relaxation, increases the probability of repeating the round trip between two neighboring temperatures. Therefore, although the P_{acc} values were similar for both τ conditions, the time required for a round trip in the temperature space differed. Similarly, frequent back exchanges were also reported by Periole & Mark for short t_{att} [19]. Second, a linear relationship between the logarithm of t_{acc} and that of t_{round} was also observed for τ=0.2 ps (Fig. 1B). Third, the α- and 3_{10}-helix contents for the two τ conditions showed similar profiles (Fig. 2 and Supplementary Fig. S1). However, some differences can be found in their potential energy distributions. For τ=0.2 ps and N_{rep}=32, the distributions of V_1 were similar for the various t_{att} settings (Fig. 3E), in contrast to the distributions when τ=2 ps (Fig. 3B). Fourth, although the thermostatting errors at T_k=300 K for the lowest t_{att} values were also observed for τ=0.2 ps, the errors were smaller than those for τ=2 ps (Fig. 4). However, an oscillation of the averaged temperatures was also observed (Fig. 5). In summary, the coupling time constant τ significantly affected the sampling efficiency and the ensemble generated by the REMD method, especially for short time intervals between the replica-exchange attempts. This suggests that artifacts arising from short t_{att} are related to insufficient thermal relaxation.

Conclusion

We evaluated the effects of parameters on REMD simulations, i.e., the number of replicas (N_{rep}), the time interval between replica-exchange attempts (t_{att}), and the coupling time constant for the thermostat (τ), in terms of the sampling efficiency and resultant ensembles of an alanine octapeptide. The results suggest that, although shorter t_{att} enhance traversals in the temperature space (Table 2), they also cause larger artifacts. Short t_{att} also shift the temperature distributions of the simulated ensembles from the target temperature of the thermostat (Fig. 4). In addition, the thermostatting errors artificially oscillate along with the thermostat-ID, *k* (Fig. 5). The potential energy distribution and helix content are also impacted by the value of t_{att} (Figs. 2 and 3). The other parameters, N_{rep} and τ, also significantly influence the generated ensembles whenever short time intervals are used.

N_{rep} is a key parameter that affects the sampling efficiency, which is measured by the time needed for a round trip in the temperature space (t_{round}). Higher N_{rep} increase both the acceptance ratio (P_{acc}; Table 1) and the acceptance number required for a round trip; the former increases and the latter decreases the efficiency. In the molecular system studied here, N_{rep}=12 or 16 show the best performance in terms of

t_{round} unless t_{att} is too short (Table 2). Although higher N_{rep} require higher computational costs, those are not always effective to enhance the sampling. The logarithm of t_{round} is proportional to that of t_{acc} (Fig. 1), and higher N_{rep} result in larger t_{round} for the same time interval for accepting the replica-exchange attempts (t_{acc}).

Whereas various combinations of parameters were examined in this study, there are some other factors which can affect the results of REMD simulations, e.g., the system size, the degree of freedom of the system, the integration time step Δt, and the thermostatting algorithm. Note that Sindhikara *et al.* examined the effects of parameters with implicit and explicit solvents and got the same conclusions in both cases. The complexity of the method makes it difficult to determine optimal parameters, and it is not straightforward to find a universal rule for the parameter determination. Although Sindhikara *et al.* recommended 10–100 steps for the replica-exchange interval [23], our results imply that this setting is not always adequate. We demonstrated that employing a 10-steps interval (t_{att}=0.01 ps) generated artifacts. Whereas using a 100-steps interval (t_{att}=0.1 ps) clearly reduced the artifacts compared with shorter intervals, the ensemble still deviated from that obtained with a 1,000-steps interval (t_{att}=1 ps). Users should carefully choose this value to get a balance between sampling efficiency and tolerable artifacts.

Conflicts of Interest

R. I., K. K., and T. T. declare that they have no conflict of interest.

Author Contribution

K. K. and T. T. designed this work. R. I. performed calculations and analyzed data. R. I., K. K., and T. T. wrote the manuscript.

References

[1] Ganesan, A., Coote, M. L. & Barakat, K. Molecular dynamics-driven drug discovery: leaping forward with confidence. *Drug Discov. Today* **22**, 249–269 (2017).

[2] De Vivo, M., Masetti, M., Bottegoni, G. & Cavalli, A. Role of Molecular Dynamics and Related Methods in Drug Discovery. *J. Med. Chem.* **59**, 4035–4061 (2016).

[3] Salomon-Ferrer, R., Götz, A. W., Poole, D., Le Grand, S. & Walker, R. C. Routine Microsecond Molecular Dynamics Simulations with AMBER on GPUs. 2. Explicit Solvent Particle Mesh Ewald. *J. Chem. Theory Comput.* **9**, 3878–3888 (2013).

[4] Shaw, D. E., Grossman, J. P., Bank, J. A., Batson, B., Butts, J. A., Chao, J. C., *et al.* Anton 2: raising the bar for performance and programmability in a special-purpose molecular dynamics supercomputer. *Proceeding of the International Conference for High Performance Computing, Networking, Storage and Analysis* 41–53 (2014).

[5] Clarke, D. T., Doig, A. J., Stapley, B. J. & Jones, G. R. The alpha-helix folds on the millisecond time scale. *Proc. Natl. Acad. Sci. USA* **96**, 7232–7237 (1999).

[6] Lindorff-Larsen, K., Piana, S., Dror, R. O. & Shaw, D. E. How Fast-Folding Proteins Fold. *Science* **334**, 517–520 (2011).

[7] Shaw, D. E. 166 Millisecond-long molecular dynamics simulations of proteins on a special-purpose machine. *J. Biomol. Struct. Dyn.* **31**, 108–108 (2013).

[8] Higo, J., Ikebe, J., Kamiya, N. & Nakamura, H. Enhanced and effective conformational sampling of protein molecular systems for their free energy landscapes. *Biophys. Rev.* **4**, 27–44 (2012).

[9] Kasahara, K., Ma, B., Goto, K., Dasgupta, B., Higo, J., Fukuda, I., *et al.* myPresto/omegagene: a GPU-accelerated molecular dynamics simulator tailored for enhanced conformational sampling methods with a non-Ewald electrostatic scheme. *Biophys. Physicobiol.* **13**, 209–216 (2016).

[10] Sugita, Y. & Okamoto, Y. Replica-exchange molecular dynamics method for protein folding. *Chem. Phys. Lett.* **314**, 141–151 (1999).

[11] Souaille, M. & Roux, B. Extension to the weighted histogram analysis method: combining umbrella sampling with free energy calculations. *Comput. Phys. Commun.* **135**, 40–57 (2001).

[12] Shirts, M. R. & Chodera, J. D. Statistically optimal analysis of samples from multiple equilibrium states. *J. Chem. Phys.* **129**, 124105 (2008).

[13] Fukunishi, H., Watanabe, O. & Takada, S. On the Hamiltonian replica exchange method for efficient sampling of biomolecular systems: Application to protein structure prediction. *J. Chem. Phys.* **116**, 9058 (2002).

[14] Mori, T., Jung, J. & Sugita, Y. Surface-Tension Replica-Exchange Molecular Dynamics Method for Enhanced Sampling of Biological Membrane Systems. *J. Chem. Theory Comput.* **9**, 5629–5640 (2013).

[15] Denschlag, R., Lingenheil, M., Tavan, P. & Mathias, G. Simulated Solute Tempering. *J. Chem. Theory Comput.* **5**, 2847–2857 (2009).

[16] Terakawa, T., Kameda, T. & Takada, S. On easy implementation of a variant of the replica exchange with solute tempering in GROMACS. *J. Comput. Chem.* **32**, 1228–1234 (2011).

[17] Nagai, T., Pantelopulos, G. A., Takahashi, T. & Straub, J. E. On the use of mass scaling for stable and efficient simulated tempering with molecular dynamics. *J. Comput. Chem.* **37**, 2017–2028 (2016).

[18] Ostermeir, K. & Zacharias, M. Advanced replica-exchange sampling to study the flexibility and plasticity of peptides and proteins. *Biochim. Biophys. Acta* **1834**, 847–853 (2013).

[19] Periole, X. & Mark, A. E. Convergence and sampling efficiency in replica exchange simulations of peptide folding in explicit solvent. *J. Chem. Phys.* **126**, 014903 (2007).

[20] Abraham, M. J. & Gready, J. E. Ensuring Mixing Efficiency of Replica-Exchange Molecular Dynamics Simulations. *J. Chem. Theory Comput.* **4**, 1119–1128 (2008).

[21] Jani, V., Sonavane, U. B. & Joshi, R. REMD and umbrella sampling simulations to probe the energy barrier of the folding pathways of engrailed homeodomain. *J. Mol. Model.* **20**, 2283 (2014).

[22] Sindhikara, D., Meng, Y. & Roitberg, A. E. Exchange frequency in replica exchange molecular dynamics. *J. Chem. Phys.* **128**, 024103 (2008).

[23] Sindhikara, D. J., Emerson, D. J. & Roitberg, A. E. Exchange Often and Properly in Replica Exchange Molecular Dynamics. *J. Chem. Theory Comput.* **6**, 2804–2808 (2010).

[24] Rosta, E. & Hummer, G. Error and efficiency of replica exchange molecular dynamics simulations. *J. Chem. Phys.* **131**, 165102 (2009).

[25] Hornak, V., Abel, R., Okur, A., Strockbine, B., Roitberg, A. & Simmerling, C. Comparison of multiple Amber force fields

and development of improved protein backbone parameters. *Proteins* **65**, 712–725 (2006).
[26] Onufriev, A., Bashford, D. & Case, D. A. Exploring protein native states and large-scale conformational changes with a modified generalized born model. *Proteins* **55**, 383–394 (2004).
[27] Hess, B., Bekker, H., Berendsen, H. J. C. & Fraaije, J. G. E. M. LINCS: a linear constraint solver for molecular simulations. *J. Comput. Chem.* **18**, 1463–1472 (1997).
[28] Hess, B. P-LINCS: A Parallel Linear Constraint Solver for Molecular Simulation. *J. Chem. Theory Comput.* **4**, 116–122 (2008).
[29] Nosé, S. A molecular dynamics method for simulations in the canonical ensemble. *Mol. Phys.* **52**, 255–268 (1984).
[30] Hoover, W. Canonical dynamics: Equilibrium phase-space distributions. *Phys. Rev. A Gen. Phys.* **31**, 1695–1697 (1985).
[31] Pronk, S., Páll, S., Schulz, R., Larsson, P., Bjelkmar, P., Apostolov, R., *et al.* GROMACS 4.5: a high-throughput and highly parallel open source molecular simulation toolkit. *Bioinformatics* **29**, 845–854 (2013).
[32] Mori, Y. & Okamoto, Y. Replica-Exchange Molecular Dynamics Simulations for Various Constant Temperature Algorithms. *J. Physical. Soc. Japan* **79**, 074001 (2010).
[33] Kabsch, W. & Sander, C. Dictionary of protein secondary structure: Pattern recognition of hydrogen-bonded and geometrical features. *Biopolymers* **22**, 2577–2637 (1983).
[34] Shi, Z., Olson, C. A., Rose, G. D., Baldwin, R. L. & Kallenbach, N. R. Polyproline II structure in a sequence of seven alanine residues. *Proc. Natl. Acad. Sci. USA* **99**, 9190–9195 (2002).
[35] Maffucci, I. & Contini, A. An Updated Test of AMBER Force Fields and Implicit Solvent Models in Predicting the Secondary Structure of Helical, β-Hairpin, and Intrinsically Disordered Peptides. *J. Chem. Theory Comput.* **12**, 714–727 (2016).
[36] Piana, S., Donchev, A. G., Robustelli, P. & Shaw, D. E. Water Dispersion Interactions Strongly Influence Simulated Structural Properties of Disordered Protein States. *J. Phys. Chem. B* **119**, 5113–5123 (2015).
[37] Henriques, J. & Skepö, M. Molecular Dynamics Simulations of Intrinsically Disordered Proteins: On the Accuracy of the TIP4P-D Water Model and the Representativeness of Protein Disorder Models. *J. Chem. Theory Comput.* **12**, 3407–3415 (2016).
[38] Weber, W., Hünenberger, P. H. & McCammon, J. A. Molecular Dynamics Simulations of a Polyalanine Octapeptide under Ewald Boundary Conditions: Influence of Artificial Periodicity on Peptide Conformation. *J. Phys. Chem. B* **104**, 3668–3675 (2000).
[39] Kastenholz, M. A. & Hünenberger, P. H. Influence of Artificial Periodicity and Ionic Strength in Molecular Dynamics Simulations of Charged Biomolecules Employing Lattice-Sum Methods. *J. Phys. Chem. B* **108**, 774–788 (2004).
[40] Reif, M. M., Kräutler, V., Kastenholz, M. A., Daura, X. & Hünenberger, P. H. Molecular Dynamics Simulations of a Reversibly Folding β-Heptapeptide in Methanol: Influence of the Treatment of Long-Range Electrostatic Interactions. *J. Phys. Chem. B* **113**, 3112–3128 (2009).
[41] Kasahara, K., Sakuraba, S. & Fukuda, I. Enhanced Sampling of Molecular Dynamics Simulations of a Polyalanine Octapeptide: Effects of the Periodic Boundary Conditions on Peptide Conformation. *J. Phys. Chem. B* **122**, 2495–2503 (2018).
[42] Greenfield, N. J. Using circular dichroism spectra to estimate protein secondary structure. *Nat. Protoc.* **1**, 2876–2890 (2007).